HHS Public Access

Author manuscript

Nat Microbiol. Author manuscript; available in PMC 2021 August 03.

Published in final edited form as:

Nat Microbiol. 2021 January ; 6(1): 44–50. doi:10.1038/s41564-020-00810-x.

Transcriptional Regulator Induced Phenotype screen reveals drug potentiators in *Mycobacterium tuberculosis*

Shuyi Ma[1,2], **Robert Morrison**[1], **Samuel J. Hobbs**[2], **Vijay Soni**[3,4], **Jessica Farrow-Johnson**[1,2], **Andrew Frando**[2,5], **Neil Fleck**[2,5], **Christoph Grundner**[2,5], **Kyu Y. Rhee**[3,4], **Tige R. Rustad**[2], **David R. Sherman**[1,2,*]

[1]Department of Microbiology, University of Washington, Seattle, Washington, 98109, USA.

[2]Interdisciplinary Program of Pathobiology, Department of Global Health, University of Washington, Seattle, Washington 98195, USA.

[3]Division of Infectious Diseases, Department of Medicine, Weill Cornell Medical College, New York, NY, 10065, USA.

[4]Department of Microbiology & Immunology, Weill Cornell Medical College, New York, NY, 10065, USA.

[5]Center for Global Infectious Disease Research, Seattle Children's Research Institute, Seattle, Washington 98109, USA

Abstract

Transposon-based strategies provide a powerful and unbiased way to study bacterial stress response[1–8], but these approaches cannot fully capture the complexities of network-based behavior. Here, we present a network-based genetic screening approach: the Transcriptional Regulator Induced Phenotype (TRIP) screen, which we used to identify previously uncharacterized network adaptations of *Mycobacterium tuberculosis* (Mtb) to the first-line anti-TB drug isoniazid (INH). We found regulators that alter INH susceptibility when induced, several of which could not be identified by standard gene disruption approaches. We then focused on a specific regulator, *mce3R*, which potentiated INH activity when induced. We compared *mce3R*-regulated genes with baseline INH transcriptional responses and implicated the gene *ctpD* (Rv1469) as a putative INH effector. Evaluating a *ctpD* disruption mutant demonstrated a previously unknown role for this gene in INH susceptibility. Integrating TRIP screening with network information can uncover sophisticated molecular response programs.

*Correspondence to: David R. Sherman (dsherman@uw.edu).

Author Contributions:

S.M. conceived of the study, led the design, generated data, analyzed the results, and drafted the manuscript. R.M. developed the software to convert raw sequencing data into abundance values for each TFI strain. S.H. generated data and assembled the pooled TFI library cultures. J.F. assisted with sample preparation for sequencing. V.S. and K.R. generated, analyzed, and interpreted the metabolite profiling data. A.F., N.F., and C.G., generated the CRISPRi strain. T.R. and D.S. conceived of the study, led the design, organized the data analysis, and drafted the manuscript.

Competing Interests:

The authors declare no competing interests.

Deciphering molecular stress response is important to studies of microbes including *Mycobacterium tuberculosis* (Mtb), the causative pathogen of tuberculosis[9]. Prolonged therapy and unfavorable outcomes arise partially because Mtb can persist in otherwise inhibitory drug concentrations by means independent of heritable resistance mutations[10–12]. Defining these adaptations can reveal biology, including unexplored drug targets and treatment-enhancing strategies. Screens of transposon-mediated gene disruption mutant pools[1–8] are powerful tools to identify candidate effector genes, but they also pose limitations: 1) they cannot identify genes whose upregulation elicits a phenotype, 2) essential genes are lost from experiments, and 3) they miss phenotypes from the coordinated actions of multiple genes. To address these limitations, we developed the Transcriptional Regulator Induced Phenotype (TRIP) screen, which quantifies growth associated with individually inducing each Mtb transcription factor (TF). TRIP offers several advantages: 1) emergent phenotypes are accessible, since regulons generally include multiple genes selected for co-regulation by evolution; 2) revealed phenotypes can be deconstructed with the existing baseline regulatory network; 3) TF expression is chemically triggered, enabling context-specific interrogation of perturbations; and 4) essential regulators and effector genes can be assessed. Thus, TRIP is highly complementary to gene disruption-based screening approaches.

TRIP exploits a library of 207 TF-induction (TFI) strains, representing 97% of annotated Mtb regulators, each transformed with a plasmid carrying a TF under control of a chemically-inducible promoter (Figure 1). Each strain is engineered for conditional induction of a single TF and expression of its associated regulon—the set of genes whose expression changes when that TF is induced [13–15]. ChIP-seq and expression profiling of TFI strains under *in vitro* log-phase conditions revealed a baseline network of transcriptional impacts and DNA binding interactions triggered by each TF [13–15].

Here, we pool the TFI library for simultaneous growth measurements (Figure 1). The pool is exposed to a stress condition either with or without TF induction. The proportion of each TFI strain in the pool is quantified by next-generation sequencing of a DNA segment unique to each strain. Sampling the pool over time generates simultaneous abundance curves for each TFI strain. The abundance fold change of each strain when induced versus uninduced identifies regulons with altered growth or survival.

We first applied TRIP to Mtb log-phase growth *in vitro* to characterize network perturbations that alter baseline fitness. Figure 2A visualizes abundance fold change of each TFI strain when induced under these conditions (Table S1 has detailed results and individual replicate data). Most TFI strains showed no significant abundance difference upon induction (Figure 2B shows an example TFI strain in this category). Twenty-two TFI strains (10.6%; below dotted line at −0.5) exhibited growth defects upon TF induction (Figure 2C shows an example TFI strain in this category).

Growth-defective strains are enriched in TFs that activate genes associated with starvation responses (Table S2). Such strains are also enriched for TFs that repress essential genes ($p < 10^{-6}$, hypergeometric test), although two defect-inducing TFIs (Rv3765c and Rv1255c) do not repress any essential genes, and 20 TFIs with no discernable growth phenotype do

repress essential genes [3]. There is no significant correlation between the number of repressed essential genes and extent of growth defect incurred by the TFI strain, which could potentially arise for several reasons, including synthetic rescues[16,17], or the nonlinear relationship between expression level and fitness for some essential genes[18].

To validate relative abundance differences detected by TRIP, we compared screening results with growth of each individual TFI strain over a one-week time course with and without TF induction. Of the 22 TFIs with strong growth defects in TRIP, 20 also had strong growth defects when cultured individually. Out of 174 other TFs with no TRIP-associated defect, only 1 TFI strain elicited greater than 1.5-fold increase in doubling time when TF expression was induced in monoculture. Notably, these 174 TFI strains included 23 TFs that we had previously characterized to elicit no transcriptional change when induced under log-phase growing conditions. These validations indicate that: 1) phenotypes detected by TRIP reflect growth observed in monoculture, 2) significant growth defect upon TF induction is uncommon and TF-specific, and 3) protein (and TF) overexpression do not convey non-specific growth defects.

With baseline Mtb network phenotypes established, we applied TRIP to study response to the frontline anti-TB agent isoniazid (INH). We exposed TFI pools to an INH dose where the bulk population grew suboptimally (19% of untreated, Extended Data 1), enabling identification of TFIs with either reduced or improved viability compared to the population average from a single experiment. Figure 2D shows the abundance of TFI strains exposed to drug when induced relative to uninduced. Strains with significant INH phenotypes partition into three groups: A) TFIs conveying growth advantage in INH but no change when untreated (6 strains, purple box); B) TFIs conveying growth defect in INH but no change when untreated (4 strains, blue box); and C) TFIs conveying growth defect in INH and untreated conditions (9 strains; light blue box). Of the 20 TFs that yield INH TRIP phenotypes, two were revealed by Tn-seq to alter Mtb fitness significantly during INH treatment (Table S2) [19]. The regulons of TFs in all three groups were enriched for genes reported to alter INH fitness by Tn-seq (Table S3) [19]. Notably, two of the four TFs in group B solely activate genes when induced (Rv0330c and Rv2282c), so association between genes in these regulons and INH fitness could not have been detected by disruption-based assays.

The TFI conveying the greatest TRIP advantage in INH is *furA* (Rv1909c). This TF represses expression of *katG* (Rv1908c), which encodes the catalase-peroxidase that converts the INH prodrug into its active form [20,21]. Inducing *furA* is known to restore nearly uninhibited growth in INH [14,20,22].

We next investigated regulons representing potential therapeutic targets. The TF conveying the greatest INH TRIP defect is *mce3R* (Rv1963c), a TetR-like regulator. *mce3R* has been linked to the expression of genes that mediate β-oxidation of fatty acids and lipid transport [23–25] and had no previous connection to INH.

To validate hypersusceptibility, we tested viability of the *mce3R* induction strain ($mce3R_{ind}$) in monoculture with INH. First, we exposed $mce3R_{ind}$ to INH, with and without TF

induction (Figure 2E). We confirmed *mce3R* induction by qPCR (Extended Data 2), and observed a significant, 4-fold additional survival defect by 7 days of INH. By day 14, during the Mtb growth rebound phase mediated by INH degradation in the culture media[26–28], the additional *mce3R* defect was 21-fold. We suspect that this is because many common *katG* mutations still retain some catalase activity and INH sensitivity[29], though we have not precluded other possible explanations. We also assayed Mtb ATP levels (BacTiter Glo, Promega, Madison, WI) after 7 days with varying INH doses (Figure 2F, Extended Data 3). We found that at every non-zero INH concentration tested, *mce3R* induction resulted in significantly lower metabolic viability, demonstrating that *mce3R*-mediated hypersusceptibility is independent of drug dose.

Hypersusceptibility could stem from TFI-mediated countering of the Mtb adaptation to INH. To investigate this hypothesis, we compared the *mce3R* induction regulon from our basal transcriptional network with genes previously shown to be differentially expressed when H37Rv is exposed to INH[14,30,31]. *ctpD* (Rv1469) is one of two genes repressed by *mce3R* (Figure 3A, see Extended Data 4 for full set), and is normally upregulated in response to INH in broth culture and under macrophage infection conditions [30,31]. After excluding the other gene (see Table S4 and Table S5 for details), we hypothesized that *ctpD* induction might be important for temporary Mtb adaptation to INH. If so, depleting *ctpD* might elicit INH hypersusceptiblity independently from *mce3R*.

To test if *ctpD* influences INH susceptibility, we obtained a transposon mutant that disrupted *ctpD* (*ctpD*::Himar1). We compared kill curves for *ctpD*::Himar1 vs. the parent strain CDC1551 when exposed to INH (Figure 3B, Extended Data 5). As predicted, *ctpD*::Himar1 survival was reduced relative to CDC1551 following INH (93-fold difference after 7 days, $p \sim 3\times10^{-5}$, t-test), with no significant growth difference without drug. To independently validate this INH hypersusceptibility, we performed a CRISPRi-mediated knockdown of *ctpD* in H37Rv. Without ATc, *ctpD* expression in the CRISPRi strain is 15% of H37Rv, and it exhibits a 95-fold CFU reduction relative to H37Rv at 7 days of INH. With ATc supplementation, *ctpD* expression in the CRISPRi strain is 8% of H37Rv, and it exhibits a 275-fold CFU reduction relative to H37Rv at 7 days of INH (Extended Data 5, see Methods for CRISPRi details). We also found that inducing *mce3R* expression in the *ctpD*::Himar1 strain conveyed greater CFU decrease at 7 days of INH treatment than the *ctpD*::Himar1 strain alone (Extended Data 6). This suggests that additional components of the *mce3R* regulon also contribute to INH sensitivity. Transcriptome profiling[14] revealed no significant expression change in the thioredoxin genes *trxA* (Rv1470) and *trxB1* (Rv1471) upon *mce3R* induction ($p > 0.3$, t-test), suggesting that polar effects on the genes downstream of *ctpD* are unlikely to contribute significantly to the INH susceptibility phenotype.

The *ctpD* gene encodes a membrane protein[32] annotated as the Mtb paralog of CtpD, a member of the metal cation-transporting P1B4-ATPase subgroup, and is essential for Mtb survival in the host [2,33,34]. CtpD is a high-affinity Fe^{2+} exporter needed to overcome redox stress and adapt to the host [33,35]. Given that KatG-mediated catalysis is iron-dependent, Fe^{2+} accumulation from *ctpD* loss could possibly increase levels of oxy-ferrous KatG, which in turn could increase INH activation [36]. Consistent with this hypothesis, metabolic profiling of the *ctpD*::Himar1 and $mce3R_{ind}$ strains showed increased intracellular accumulation of INH

and activated INH-NAD adduct[37] (Figure 3C, Extended Data 7). Notably, *mce3R* induction in *ctpD*::Himar1 does not convey additional INH-NAD adduct accumulation, suggesting that *ctpD* is a major contributor of *mce3R*-mediated modulation of INH activation. Alternatively, extra free iron in Mtb could promote cell wall changes [19] or increased oxidative stress [38] that may enhance INH activity. RNA-seq transcriptome profiling of the *ctpD*::Himar1 strain indicates that *katG* expression is ~1.7-fold higher and *furA* expression is ~2.1 fold higher than wildtype after 1 day of INH ($p < 0.01$, t-test). Given the aforementioned link between *furA* and *katG* [14,20,22], it possible that the *ctpD*-mediated phenotype is partially mediated by *katG* expression change. Further work is needed to establish the mechanism of CtpD-mediated intrinsic INH susceptibility, and whether this mechanism extends to other cation transmembrane transporters.

TRIP represents a powerful tool to unravel the links between genetic perturbations and their phenotypic outcomes under various environmental contexts. Previous TF-centric strategies profiled individual TF perturbation strains separately, requiring up to hundreds of cultures to capture regulatory fitness in a single condition[14,31,39,40]. In contrast, TRIP enables parallelized fitness quantification across Mtb TFs within a single culture. TRIP can reveal associations between genes, networks, and fitness in several ways. First, by targeting regulons, TRIP harnesses nature's levers to modulate responses—tuning gene sets that evolved to change coordinately—and uncovers phenotypes that depend on synchronized actions of multiple genes. For example, two TFIs that slowed growth under log-phase conditions (Rv3765c and Rv1255c) do not repress any essential genes, suggesting that epistatic mechanisms may underlie these defects. Second, TRIP samples network states distinct from those elicited by TF disruption. For example, *mce3R* was previously reported to regulate the *mce3* operon genes based on studies of a deletion mutant [23,24]. However, the transcriptional impact of inducing *mce3R* does not include the *mce3* operon (Table S2 shows full regulon, based on [14]), suggesting that *mce3R* participates in complex regulatory circuits. Combining gene disruption studies with TRIP and network analysis could facilitate deconstructing these nonlinear effects. Finally, unlike gene disruption assays, TRIP can profile upregulation phenotypes, as with the INH hypersusceptibility-inducing TFs Rv0330c and Rv2282c, both of which exclusively activate genes.

In this study, we combined TRIP with network analysis to identify genes that altered Mtb response to INH. However, TRIP can interrogate network mediators of fitness under any condition from which microbes can be recovered, and TRIP requires tracking a substantially reduced set of mutants compared to Tn-seq, rendering it technically tractable. By integrating with network information, TRIP will lend insights into emergent mechanisms underlying condition-specific growth phenotypes in Mtb, and the strategy can be generalized for other organisms.

Methods:

Strains and expression vectors.

The individual strains comprising the Mtb Transcription Factor Induction (TFI) Library were generated previously [14]. Briefly, 207 Mtb DNA binding genes were cloned into a tagged, inducible vector that placed the TF under control of a tetracycline-inducible promoter and

added a C-terminal FLAG epitope tag [14,41–44]. The constructs were then individually transformed into Mtb H37Rv using standard methods. Individual TFI strains are available from the BEI strain repository at ATCC ([45], NR-46512). The TFI library was generated by combining equal proportions of each strain into a common pool.

The *ctpD* transposon strain (*ctpD*::Himar1) was obtained through BEI Resources, NIAID, NIH: Mtb: Strain CDC1551, Transposon Mutant 1738 (MT1515, Rv1469), NR-18218 [45]. The transposon insertion is located at base 671 in the 1974 base-pair long gene [45]. To trigger *mce3R* induction in this strain, we transformed the *mce3R* TFI plasmid into *ctpD*::Himar1, to generate the *ctpD*::Himar1::$mce3R_{ind}$ strain. As an additional control, we also generated an $mce3R_{ind}$ (CDC1551) strain by transforming the *mce3R* TFI plasmid into the CDC1551 strain background.

The *ctpD* CRISPRi strain was constructed according to the method outlined previously in [46]. Briefly, we used the pJR965 plasmid encoding a tetracyline-inducible dCas9, a tetracycline-inducible *ctpD* -specific sgRNA, and kanamycin-selectable marker. We made the *ctpD* -specific sgRNA by annealing two complementary oligonucleotides targeting the non-template strand of the *ctpD* ORF 3' of a PAM (protospacer adjacent motif) sequence (forward primer sequence: GGGAGTTCAGTTGCGCCACTAGTCCGG; reverse primer sequence: AAACCCGGACTAGTGGCGCAACTGAAC). pJR965 was digested with BsmBI and *ctpD* -specific sgRNA was ligated into digested pJR965 using T4 DNA ligase. The ligation reaction was transformed into competent *Escherichia coli* and sgRNA insertions were confirmed by Sanger sequencing before the plasmids were transformed into Mtb.

Culture.

Bacteria were cultured at 37°C under aerobic conditions with constant agitation. For the experiments involving TFI strains, the strains were cultured in Middlebrook 7H9 with the ADC supplement (Difco), 0.05% Tween80, and 50 μg/mL hygromycin B to maintain the plasmids.

For the TRIP experiments, growth of the pooled TFI library was monitored by OD600. At an OD600 of 0.1, expression of the pooled TFI library was induced with anhydrotetracycline (ATc, 100ng/mL), and the cultures were grown for 7 days supplemented with either 3.6μM INH in 1% DMSO solution or DMSO as no-drug control. The cultures were sampled at Day 0 and Day 7 of the experiment for DNA isolation and subsequent sequencing.

For individual TFI strain time course experiments, each strain was cultured under the same media conditions as described for the pooled TFI library. When cultures reached OD600 ~0.1, TFI strain induction and drug exposure proceeded as described for the pooled TFI library. The individual strain cultures were monitored for up to 14 days, with viability under the different drug and induction conditions assayed by plating on Middlebrook 7H10 solid media plates and assessing colony forming units using standard methods.

The *ctpD*::Himar1 strain was cultured in Middlebrook 7H9 with ADC supplement (Difco), 0.05% Tween80, and 30 μg/mL kanamycin to maintain the transposon insertion. Growth and survival of Rv1469 mutant was compared against the parent Mtb CDC1551 strain. When

cultures reached an OD600 of 0.1, drug exposure proceeded as described for the pooled TFI library. The individual strain cultures were monitored for up to 14 days, with viability under the different drug and induction conditions assayed by plating on Middlebrook 7H10 solid media plates and assessing colony forming units using standard methods.

To prepare for metabolomic profiling, Mtb strains were cultured at 37°C in Middlebrook 7H9 broth (BD) containing 0.2% glycerol, 0.04% Tyloxapol, 0.85g/L NaCl, 2 g/L D-glucose, and 5 g/L Fraction V BSA (Roche).

Dose-dependent viability assay.

Strains were grown to log phase (OD600 ~0.3), diluted to a final OD600 of 0.005, and dispensed into 96-well flat-bottom plates (Corning, Acton, MA) at a final volume of 200μL, containing 1% DMSO and varying concentrations of INH in the different wells. On each plate, control wells for each of the strains studied were included, containing no drug and 1% DMSO vehicle, to measure viability in the absence of INH exposure. Plates were incubated at 37°C for 7 days. Cellular viability was assayed on Day 7 by adding 20μL of culture from each well to 20μL of BacTiter-Glo Microbial Cell Viability Assay Reagent (Promega, Madison, WI), incubating at room temperature protected from direct light for 20 minutes, and reading luminescence intensity using a FluoStar Omega plate reader (BMG Lab Tech, Cary, NC).

DNA isolation and sequencing.

Cell pellets collected from each sample were resuspended in TE buffer, pH 8.0, transferred to a tube containing Lysing Matrix B (QBiogene, Inc.), and vigorously shaken three times at 6m/s for 30 seconds per cycle in a Bead Ruptor 24 homogenizer (Omni International, Kennesaw, GA), with a 30-second pause between each cycle. The mixture was centrifuged at maximum speed for one minute, and DNA was extracted from the supernatant using the MagJet Genomic DNA Kit (Thermo Fisher), according to the manufacturer's instructions for manual genomic DNA purification.

PCR pre-amplification of DNA barcodes unique to each TFI strain was performed. The products of this reaction were prepared for Illumina sequencing using the NEBNext Ultra DNA Library Prep Kit for Illumina (New England Biolabs, Ipswich, MA) according to manufacturer's instructions, and using the AMPure XP reagent (Agencourt Bioscience Corporation, Beverly, MA) for size selection and cleanup of adaptor-ligated DNA. We used the NEBNext Multiplex Oligos for Illumina (Dual Index Primers Set 1) to barcode the DNA libraries associated with each replicate and enable multiplexing of 96 libraries per sequencing run. The prepared libraries were quantified using the Kapa qPCR quantification kit, and were sequenced at the University of Washington Northwest Genomics Center with the Illumina NextSeq 500 Mid Output v2 Kit (Illumina Inc, San Diego, CA). The sequencing generated an average of 1.5 million 75 base-pair paired-end raw read counts per library.

Sequencing read alignment and TFI strain abundance deconvolution.

Read alignment was carried out using a custom processing pipeline that harnesses the Bowtie 2 utilities [47,48], which is available at A custom Bowtie 2 target index was constructed from: the CDS sequences of all H37Rv genes; the inducible TFI anchor plasmid sequence; and the complete sequence of the empty plasmid as a negative control. The two mate-pair FASTQ datasets for each sample were separately mapped as unpaired reads using Bowtie 2's local alignment mode. After both mate end datasets were aligned separately, the alignment results were combined to give a pair of gene/plasmid alignments for each raw read. Only raw read pairs having one alignment to the anchor plasmid and the other to a gene with an existing "Rv" code were kept as valid reads. Read pairs that mapped to "Rv" code genes on both ends, or pairs that failed to align were discarded. On average, each sample had 99.9% valid anchor/gene reads, which is comparable to typical RNA-seq and WGS alignment results. Libraries that generated fewer than 10,000 valid read pairs were excluded from further analysis. Valid reads were then tallied for all "Rv" code genes reported as raw abundance measures. Read counts for each TFI were then normalized as log2 reads per million (RPM) values. Higher RPM values indicated that the corresponding TFI strain had greater relative abundance in the pooled culture. The average log2 RPM values across TFIs were 11.7±3.2. TFIs with low abundance levels on day 0 of each experiment (log2 RPM < 5) were excluded from subsequent analysis (10 TFI strains, 4.8%).

We performed each TRIP experiment on two independent occasions, and included four biological replicates per condition on each occasion. To assess the effect of induction on TFI strain relative abundance, the log2 fold-change RPM values of each replicate were calculated for the TFI-induced condition relative to un-induced. These values were averaged and further normalized by the number of doublings of the pooled library estimated from the change in OD600 over the course of the experiment. Positive fold change RPM values indicated that TFI induction conveyed a growth benefit, whereas negative fold change RPM values indicated that the TFI induction conveyed a growth defect under the conditions assayed. We estimated the statistical significance of the TFI-mediated log2 fold change abundance values detected in two ways. For each TFI strain, we first calculated a z-score for each TFI-induced replicate, relative to uninduced. This is intended to assess the number of standard deviations a particular TFI-induced replicate is away from the null distribution estimated from the uninduced replicates. We calculated the z-score of the i^{th} TFI-induced replicate using the following formula: $z_i = \frac{x_{+,\,i} - \bar{x_-}}{\sigma_-}$, where $x_{+,i}$ represents the log2 RPM value for the i^{th} TFI-induced replicate, $\bar{x_-}$ represents the average log2 RPM value across uninduced TFI replicates, and σ_- represents the standard deviation of the log2 RPM values across uninduced TFI replicates. We can then summarize the z-score associated with a TF induction by averaging the z-scores calculated across induced TFI replicates. In addition to assessing significance by z-score, we also calculated p-values of log2 RPM fold change associated with each TFI strain induction by using the Student's t-test. TFI strains that exhibited a log2 fold-change per doubling greater than 0.5 with z-score greater that 1 and t-test p-value < 0.05 were deemed to have a significant growth phenotype under the condition assayed. The full z-scores and p-values for each TFI strain are reported in Table S1. The

code used to generate this processing is available at https://github.com/DavidRShermanLab/TRIPscreen.

RNA-seq transcriptome profile data generation.

To profile the Mtb transcriptome response to exposure of individual drugs, cultures were diluted to OD_{600} ~ 0.2 (equivalent to 10^8 CFU/mL) and exposed to a minimum inhibitory concentration (MIC)-equivalent dose of drug for approximately 16 hours.

RNA was isolated from these cultures and were prepared for sequencing as described previously [14,49,50]. Briefly, cell pellets in Trizol were transferred to a tube containing Lysing Matrix B (QBiogene) and vigorously shaken at maximum speed for 30 s in a FastPrep 120 homogenizer (QBiogene) three times, cooling on ice between shakes. This mixture was centrifuged at maximum speed for 1 minute, and the supernatant was transferred to a tube containing 300 μL chloroform and Heavy Phase Lock Gel (Eppendorf). This tube was inverted for 2 minutes and centrifuged at maximum speed for 5 minutes. RNA in the aqueous phase was then precipitated with 300 μL isopropanol and 300 μL high salt solution (0.8 M Na citrate, 1.2 M NaCl). RNA was purified using a RNeasy kit following the manufacturer's recommendations (Qiagen) with one on-column DNase treatment (Qiagen). Total RNA yield was quantified using a Nanodrop (Thermo Scientific).

To enrich the mRNA, ribosomal RNA was depleted from samples using the RiboZero rRNA removal (bacteria) magnetic kit (Illumina Inc, San Diego, CA). The products of this reaction were prepared for Illumina sequencing using the NEBNext Ultra RNA Library Prep Kit for Illumina (New England Biolabs, Ipswich, MA) according to manufacturer's instructions, and using the AMPure XP reagent (Agencourt Bioscience Corporation, Beverly, MA) for size selection and cleanup of adaptor-ligated DNA. We used the NEBNext Multiplex Oligos for Illumina (Dual Index Primers Set 1) to barcode the DNA libraries associated with each replicate. To achieve adequate sequencing coverage, we multiplexed 40 libraries per sequencing run. The prepared libraries were quantified using the Kapa qPCR quantification kit, and were sequenced at the University of Washington Northwest Genomics Center with the Illumina NextSeq 500 High Output v2 Kit (Illumina Inc, San Diego, CA). The sequencing generated an average of 75 million base-pair single-end raw read counts per library.

Read alignment was carried out using the previously mentioned custom processing pipeline that harnesses the Bowtie 2 utilities[47,48], available at https://github.com/robertdouglasmorrison/DuffyNGS and https://github.com/robertdouglasmorrison/DuffyTools[49]. The RNA-seq data profiling response to drug exposure generated for this study are publicly available at the Gene Expression Omnibus (GEO) at GSE151991.

Metabolite extraction.

Metabolomics experiments and analysis were performed according to published literature[51]. One milliliter of mid-log phase cultures (0.8 −1 OD580) was passed through 0.22-μm nylon filters and allowed to grow at 37°C for 5 days on Middlebrook 7H11 agar (BD) supplemented with 0.2% glycerol, 0.85g/L NaCl, 2 g/L D-glucose, and 5 g/L Fraction V BSA (Roche). On Day 6, Mtb -laden filters were transferred onto a reservoir containing 7H9

media (without tyloxapol) with 50 ng/ml ATc and left at 37°C for 24 hrs. Next, these acclimatized filters were exposed to fresh 7H9 media with and without INH (7.2 μM) and ATc. After 24 hours, these filters were quenched in precooled (−40°C) mix of acetonitrile/methanol/water (40%:40%:20%). Metabolites were extracted by bead beating using 0.1 mm Zirconia beads and Precellys homogenizer (Bertin Instruments, Rockville, MD). Lysates were centrifuged and decontaminated by passing through Spin-X tube filters tubes (0.22 μm, Sigma).

Mass spectrometry and Liquid Chromatography.

Metabolomics was performed by separating 2 μL sample on a Diamond Hybrid Type C Column (Cogent) using 1200 liquid chromatography (Agilent) coupled to an Agilent Accurate Mass 6220 Time of Flight (TOF) spectrometer. To collect all classes of metabolites, two different solvents (solvent A: water with 0.2% formic acid and solvent B: acetonitrile with 0.2% formic acid) were used at the following gradients with 0.4 mL/min of flow rate. The gradient was: 85% B: 0–2 min; 80% B: 3–5 min; 75% B: 6–7 min; 70% B: 8–9 min; 50% B: 10–11 min; 20% B: 11–14 min; 5% B: 14–24 min and 10 min of re-equilibration period using 85% B. Ion abundances of INH and INH-NAD were determined using Profinder 8.0 and Qualitative Analysis 7.0 (Agilent Technologies, USA). Standard INH and INH-NAD were used to determine the accuracy of identified peaks. Fold change was calculated with-respect to the abundances of corresponding wild type strains (H37Rv or CDC1551).

Statistics and Reproducibility.

Unless indicated, experiments were performed three times, and the mean and standard deviation from biological replicates of representative experiments are reported. Statistical differences between means were evaluated by two-tailed Student’s t-tests, statistically significant correlation was evaluated by calculating a Pearson correlation coefficient and comparing against a Student’s t distribution, and statistical enrichment was evaluated by hypergeometric test, unless otherwise noted. The significance cutoff was set at $p < 0.05$, unless otherwise indicated.

Gene Ontology Enrichment Analysis.

The gene ontology (GO) term annotations for genes comprising the regulons of the TFs under analysis were taken from [52] and evaluated for statistical enrichment against the GO annotations for the entire gene set of the Mtb strain H37Rv using the hypergeometric test and further subjected to a Bonferroni correction for multiple hypothesis testing, with the number of independent tests estimated as the number of GO terms associated to at least 2 genes in the H37Rv reference gene set (analogous to method used by [53]). We further filtered the enriched GO terms to only those featured in the regulons for 2 more of the TFs under analysis.

Data Availability.

The data reported in the paper are available in the Supplementary Materials. The raw TRIP fastq sequence data files are deposited in the Sequence Read Archive database (https://

www.ncbi.nlm.nih.gov/bioproject/PRJNA483505/). The RNAseq data are deposited in the Gene Expression Omnibus database (https://www.ncbi.nlm.nih.gov/geo/query/acc.cgi?acc=GSE151991). The Transcription Factor Induction (TFI) strains are available from BEI resources (https://www.beiresources.org/Home.aspx).

Code Availability.

The code required to process the TRIP and RNAseq sequenced reads are available at: https://github.com/robertdouglasmorrison/DuffyNGS, https://github.com/robertdouglasmorrison/DuffyTools, and https://github.com/DavidRShermanLab/TRIPscreen.

Extended Data

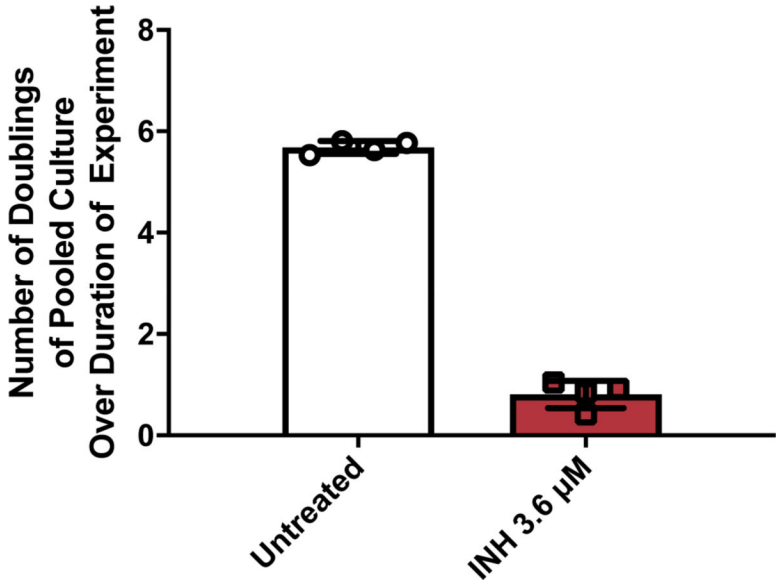

Extended Data Fig. 1. Comparing TFI pool growth between experimental conditions.
Number of doublings for TFI strain pool over duration of TRIP experiments in the untreated vs. INH treated conditions, estimated from the change of OD600 over the course of the experiment. Data show mean ± SD of four biological replicates from a representative experiment (three independent experiments were performed in total).

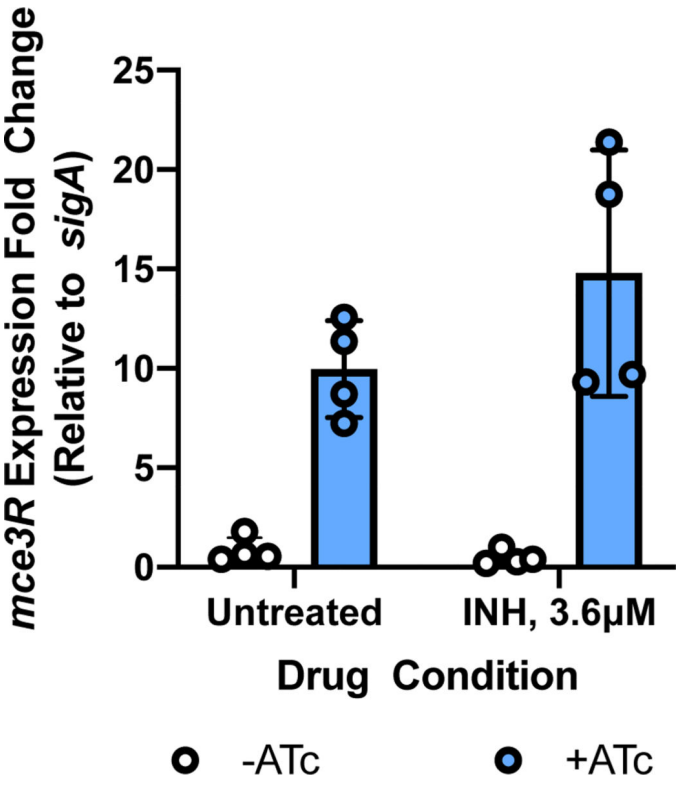

Extended Data Fig. 2. Chemical induction triggers *mce3R* expression change.

Expression fold change of *mce3R* relative to the housekeeping gene *sigA*, assessed by qPCR. Data show mean ± SD of 4 biological replicates from a representative experiment (two were performed in total). Conditions compared are in absence (white bars) and presence (black bars) of anhydrous-tetracycline (ATc) inducer, and presence and absence of INH exposure. Results show at least 8-fold activation of *mce3R* expression upon induction with ATc in both absence and presence of INH ($p = 0.00035$, two-sided t-test for −ATc untreated vs. +ATc untreated; $p = 0.0036$, two-sided t-test for −ATc + INH vs. +ATc + INH).

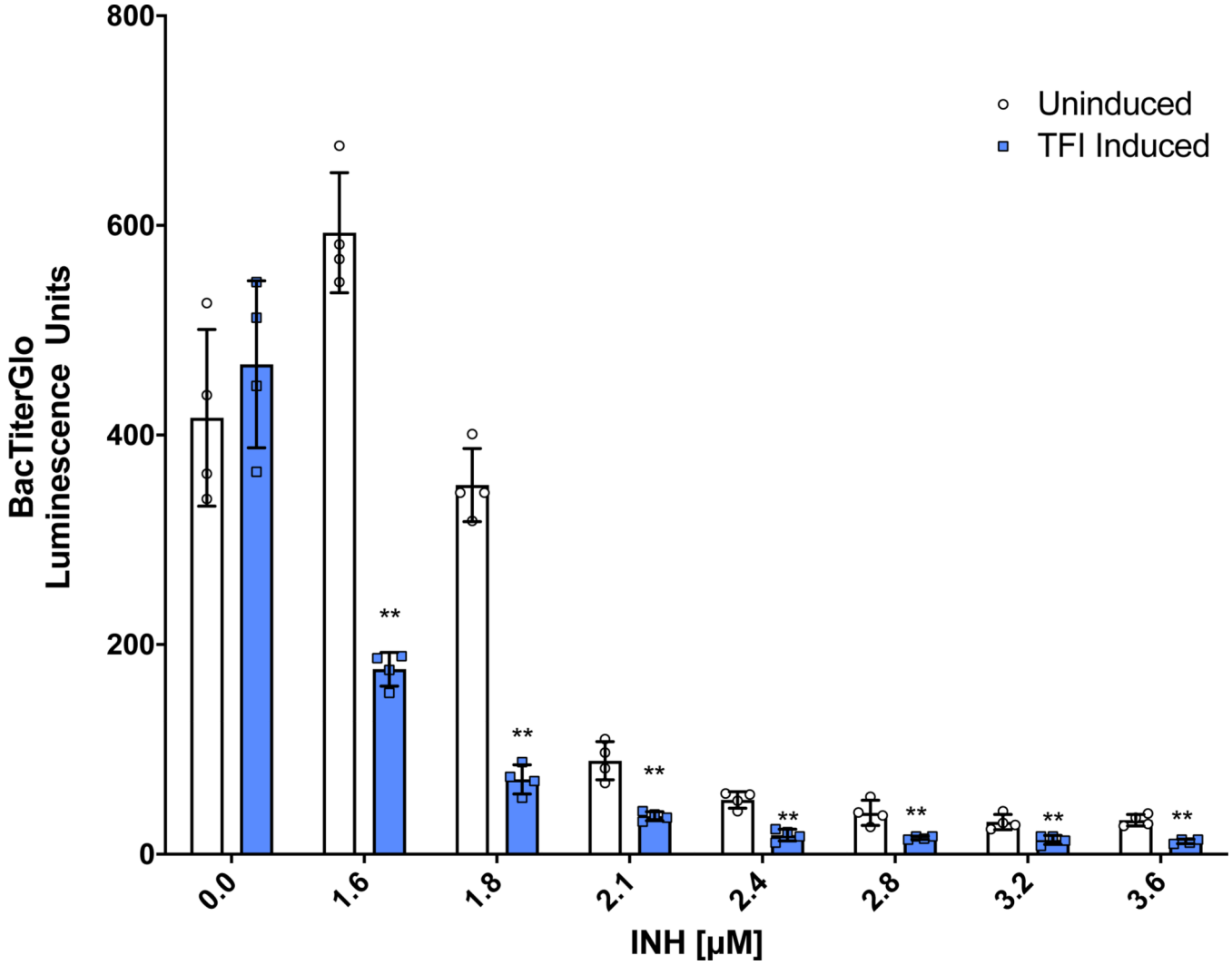

Extended Data Fig. 3. *mce3R*$_{ind}$ metabolic viability after 7 days INH.

Viability upon TFI induction (blue) is compared to uninduced (white), as measured by luminescence (see Methods). Data presented as mean Error bars show ± SD from four biological replicates. ** indicates significant differences between induction states ($p = 8.3 \times 10^{-6}$ comparing uninduced vs. TFI induced at 1.6 μM; $p = 5.7 \times 10^{-6}$ comparing uninduced vs. TFI induced at 1.8 μM; $p = 1.3 \times 10^{-3}$ comparing uninduced vs. TFI induced at 2.1 μM; $p = 4.3 \times 10^{-4}$ comparing uninduced vs. TFI induced at 2.4 μM; $p = 7.6 \times 10^{-3}$ comparing uninduced vs. TFI induced at 2.8 μM; $p = 6.9 \times 10^{-3}$ comparing uninduced vs. TFI induced at 3.2 μM; $p = 4.6 \times 10^{-4}$ comparing uninduced vs. TFI induced at 3.6 μM). Each p-value was calculated based on a two-sided t-test.

A

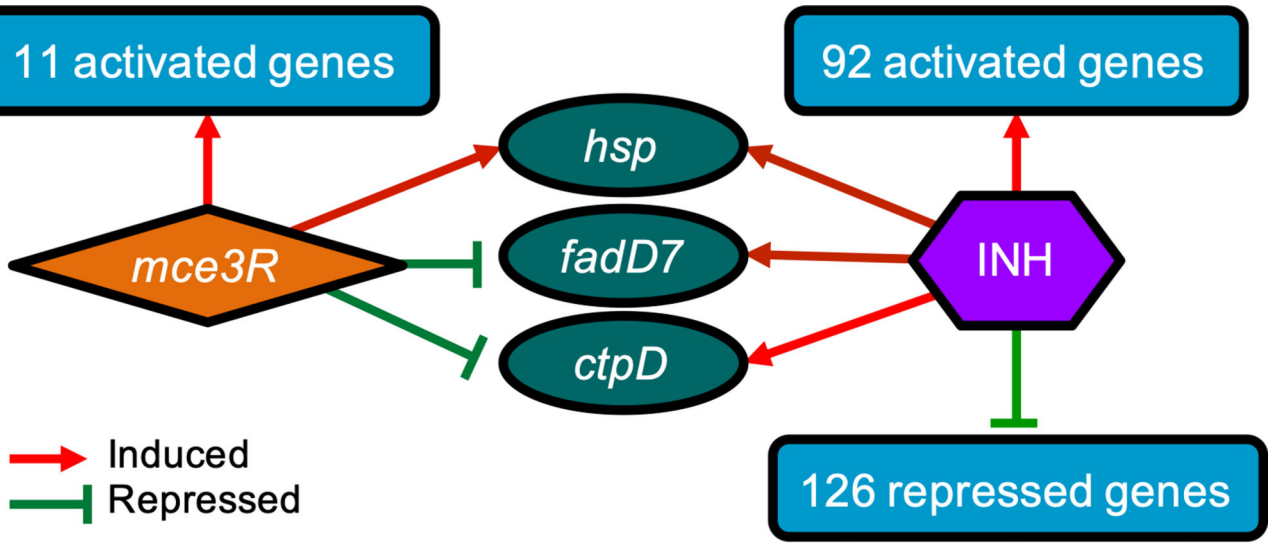

B

Target Genes	INH response log2 fold-change	*mce3R* induction response log2 fold-change
fadD7	0.88	-1.14
hsp	1	1.28
ctpD	1.99	-1.09

Extended Data Fig. 4. Overlap of genes regulated by *mce3R* that also modulate expression in baseline response to INH exposure.

(**A**) Network diagram depicts the genes differentially expressed upon induction of *mce3R* expression (left), and upon exposure to INH (right). Three genes alter expression under both these conditions. (**B**) Table summarizes the expression fold-changes of the genes perturbed both by *mce3R* induction and INH exposure.

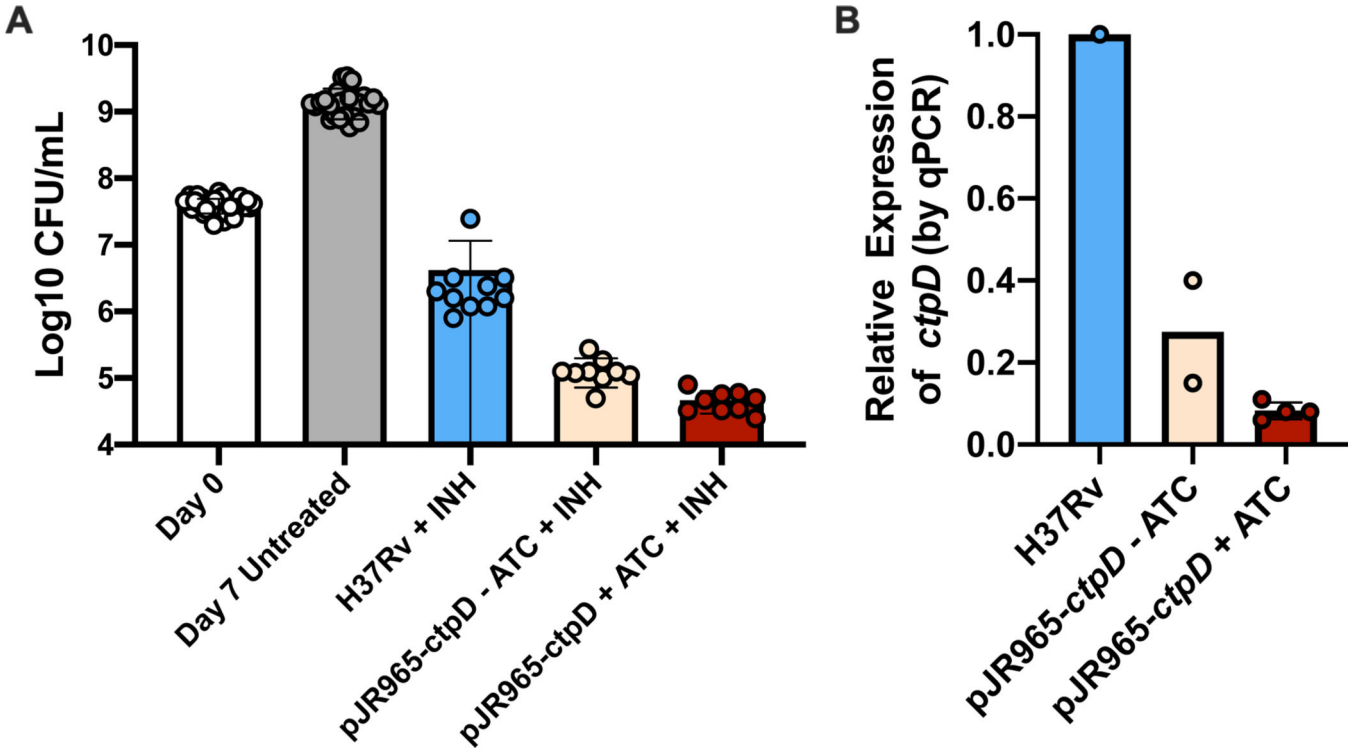

Extended Data Fig. 5. Association between *ctpD* expression and INH sensitivity.

(A) CFU/mL at 0 days and 7 days of H37Rv (black bar) and a *ctpD* CRISPRi-knockdown strain without (yellow) and with (red) chemical induction of CRISPRi activity. Both strains were exposed to 3.6μM INH or no drug. There was no significant difference between the growth of strains without drug, and the average untreated CFU/mL is plotted in the gray bar. Data show mean ± SD of three biological replicates from two independent experiments (for H37Rv conditions) or one experiment (pJR965-*ctpD* conditions). There is a significant difference between the CRISPRi knockdown and wildtype strains ($p = 0.00027$ for Day 7 H37Rv + INH vs. Day 7 pJR965-*ctpD* – ATc + INH, Wilcoxon ranksum test with continuity correction; $p = 0.00027$ for Day 7 H37Rv + INH vs. Day 7 pJR965-*ctpD* + ATc + INH, Wilcoxon ranksum test with continuity correction; $p = 0.0012$ for Day 7 pJR965-*ctpD* – ATc + INH vs. Day 7 pJR965-*ctpD* + ATc + INH, Wilcoxon ranksum test with continuity correction). **(B)** qPCR quantification of *ctpD* expression levels relative to the wildtype H37Rv in the CRISPRi knockdown strain with and without chemical induction of activity. The CRISPRi strain exhibited marked repression even in the absence of chemical induction. Data shown are from two biological replicates for the CRISPRi knockdown strain, uninduced and four biological replicates for the CRISPRi knockdown strain with induction. The experiment was performed once.

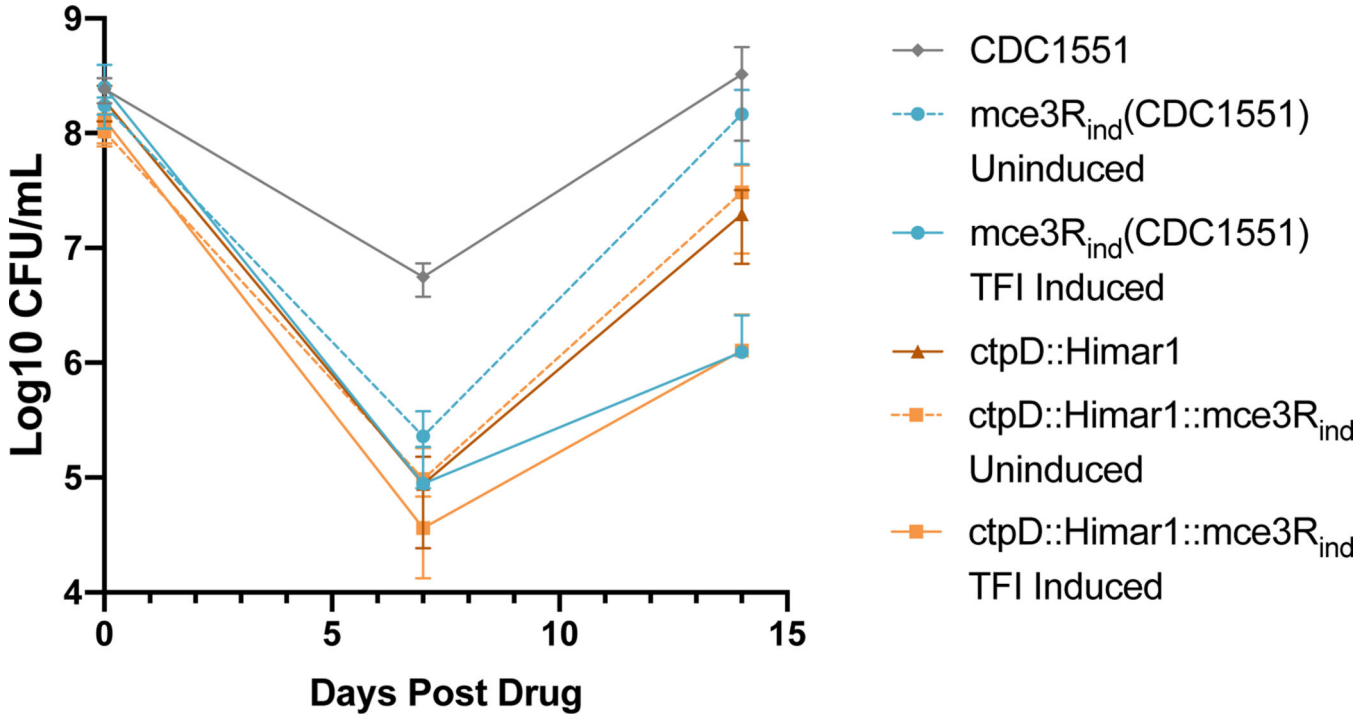

Extended Data Fig. 6. Comparing the effect of *in vitro* INH on *mce3R* and *ctpD* perturbation strains.

We measured the effect of *mce3R* induction in the CDC1551 strain background (blue) and in the *ctpD*::Himar1 strain background (orange) on Mtb survival in INH (3.6 μM), added on Day 0, as quantified by CFU/mL. Solid blue and orange lines indicate TFI induction and dashed blue and orange lines indicate TFI uninduced. As additional controls, we also compared survival of the CDC1551 wildtype strain (gray), as well as the *ctpD*::Himar1 strain (red). The data suggest that *mce3R* induction conveys significant additional fitness defect relative to *ctpD*::Himar1 strain at day 14 ($p = 0.00058$, two-sided t-test comparing *ctpD*::Himar1:: *mce3R*$_{ind}$ TFI induced vs. *ctpD*::Himar1; $p = 0.0024$, two-sided t-test comparing *mce3R*$_{ind}$ (CDC1551) TFI induced vs. CDC1551). There appears to be a modest (though not statistically significant) difference in the extent of INH-mediated killing at 7 days between the *ctpD*::Himar strain (red) and the *ctpD*::Himar1 strain with *mce3R* induction (orange solid) ($p = 0.09$, two-sided t-test). Data show mean ± SD of three biological replicates from one experiment.

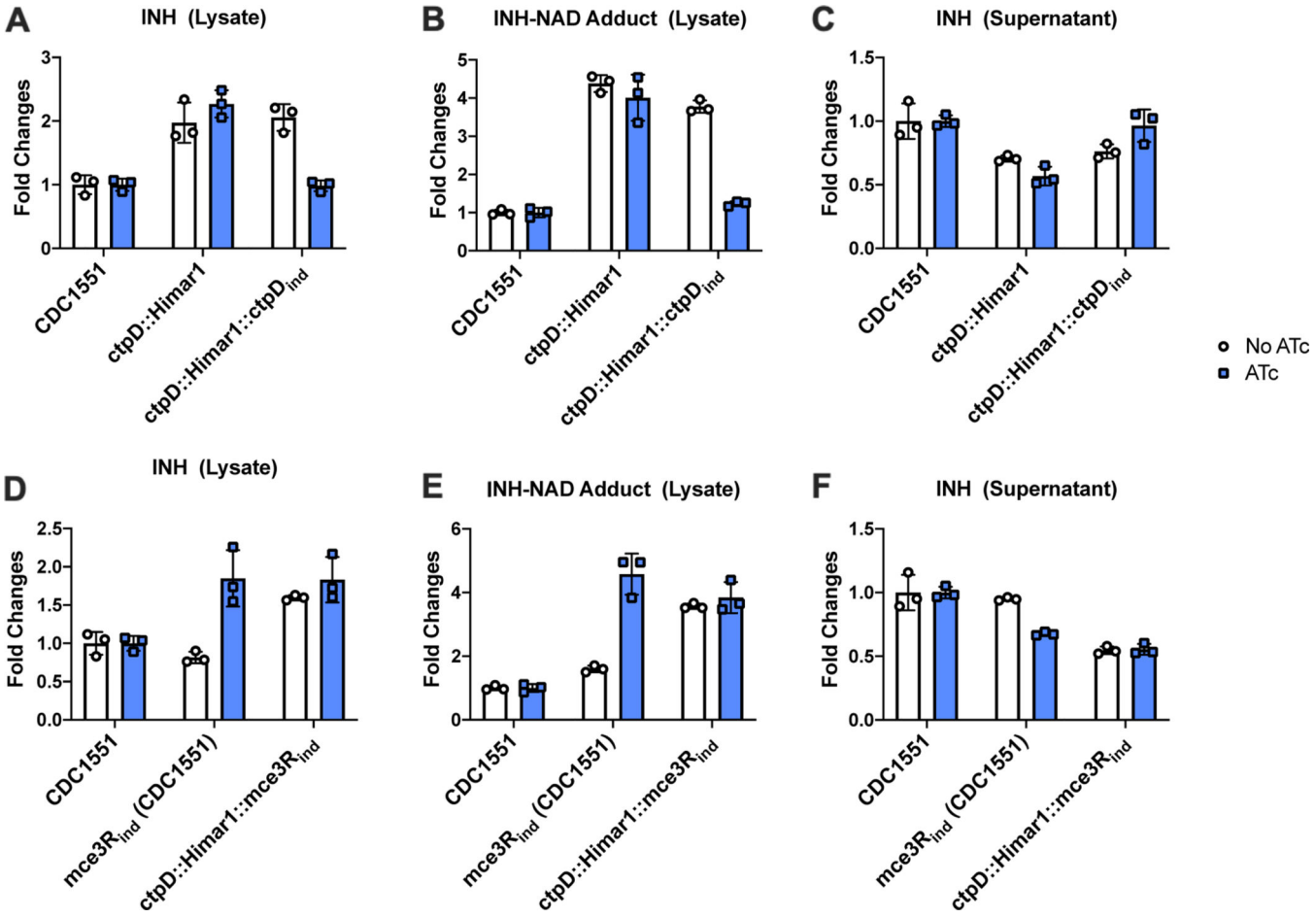

Extended Data Fig. 7. Association between *mce3R*, *ctpD* expression and abundance of INH and INH-NAD adduct during drug exposure.

Relative abundance of INH and INH-NAD adduct in Mtb lysate (panels A, B, D, E) or supernatant (panels C, F) of strains exposed to 7.2μM INH for 24 hours. Panels A, B, and C show effect of *ctpD* transposon disruption and complementation with episomally ATc-inducible *ctpD* expression. Panels D, E, and F show the effect of *mce3R* induction with or without *ctpD* transposon disruption. *ctpD* disruption conveyed increased intracellular INH and INH-NAD levels and concomitant decreased levels of INH in the supernatant. Induction of *mce3R* also increases intracellular INH and INH-NAD levels, but does not convey additional accumulation increase in the *ctpD* transposon strain background. Bars plot mean ± SD for 3 biological replicates.

Supplementary Material

Refer to Web version on PubMed Central for supplementary material.

Acknowledgments:

We gratefully acknowledge Jeremy Rock for kindly providing us with the pJR965 plasmid encoding a tetracyline-inducible dCas9 and kanamycin-selectable marker. We also thank Jessica Winkler, Jenny Lohmiller, and Reiling Liao for their technical assistance, and Susan Shen for helpful discussions.

This work was supported by the National Institutes of Health [grant numbers U 19 AI106761; U19 AI111276; U19 AI135976; 5T32AI007509].

References:

1. Sassetti CM, Boyd DH & Rubin EJ Comprehensive identification of conditionally essential genes in mycobacteria. Proc Natl Acad Sci U S A 98, 12712–12717, doi:10.1073/pnas.231275498 (2001). [PubMed: 11606763]
2. Sassetti CM & Rubin EJ Genetic requirements for mycobacterial survival during infection. Proc Natl Acad Sci U S A 100, 12989–12994, doi:10.1073/pnas.2134250100 (2003). [PubMed: 14569030]
3. Griffin JE et al. High-resolution phenotypic profiling defines genes essential for mycobacterial growth and cholesterol catabolism. PLoS Pathog 7, e1002251, doi:10.1371/journal.ppat.1002251PPATHOGENS-D-11-00689 [pii] (2011).
4. Langridge GC et al. Simultaneous assay of every Salmonella Typhi gene using one million transposon mutants. Genome Res 19, 2308–2316, doi:10.1101/gr.097097.109 (2009). [PubMed: 19826075]
5. Gallagher LA, Shendure J. & Manoil C. Genome-scale identification of resistance functions in Pseudomonas aeruginosa using Tn-seq. MBio 2, e00315–00310, doi:10.1128/mBio.00315-10 (2011). [PubMed: 21253457]
6. van Opijnen T, Bodi KL & Camilli A. Tn-seq: high-throughput parallel sequencing for fitness and genetic interaction studies in microorganisms. Nat Methods 6, 767–772, doi:10.1038/nmeth.1377 (2009). [PubMed: 19767758]
7. Goodman AL et al. Identifying genetic determinants needed to establish a human gut symbiont in its habitat. Cell Host Microbe 6, 279–289, doi:10.1016/j.chom.2009.08.003 (2009). [PubMed: 19748469]
8. Gawronski JD, Wong SM, Giannoukos G, Ward DV & Akerley BJ Tracking insertion mutants within libraries by deep sequencing and a genome-wide screen for Haemophilus genes required in the lung. Proc Natl Acad Sci U S A 106, 16422–16427, doi:10.1073/pnas.0906627106 (2009). [PubMed: 19805314]
9. WHO. Global Tuberculosis Report 2016. (2016).
10. Warner DF & Mizrahi V. Tuberculosis chemotherapy: the influence of bacillary stress and damage response pathways on drug efficacy. Clin Microbiol Rev 19, 558–570, doi:10.1128/CMR.00060-05 (2006). [PubMed: 16847086]
11. Aldridge BB, Keren I. & Fortune SM The Spectrum of Drug Susceptibility in Mycobacteria. Microbiol Spectr 2, doi:10.1128/microbiolspec.MGM2-0031-2013 (2014).
12. Wallis RS et al. Drug tolerance in Mycobacterium tuberculosis. Antimicrob Agents Chemother 43, 2600–2606 (1999). [PubMed: 10543735]
13. Minch KJ et al. The DNA-binding network of Mycobacterium tuberculosis. Nat Commun 6, 5829, doi:10.1038/ncomms6829 (2015). [PubMed: 25581030]
14. Rustad TR et al. Mapping and manipulating the Mycobacterium tuberculosis transcriptome using a transcription factor overexpression-derived regulatory network. Genome Biol 15, 502, doi:10.1186/PREACCEPT-1701638048134699 (2014). [PubMed: 25380655]
15. Galagan JE et al. The Mycobacterium tuberculosis regulatory network and hypoxia. Nature 499, 178–183, doi:nature12337 [pii] 10.1038/nature12337 (2013). [PubMed: 23823726]
16. Motter AE, Gulbahce N, Almaas E. & Barabasi AL Predicting synthetic rescues in metabolic networks. Mol Syst Biol 4, 168, doi:10.1038/msb.2008.1 (2008). [PubMed: 18277384]
17. Wytock TP et al. Experimental evolution of diverse Escherichia coli metabolic mutants identifies genetic loci for convergent adaptation of growth rate. PLoS Genet 14, e1007284, doi:10.1371/journal.pgen.1007284 (2018).
18. Wei JR et al. Depletion of antibiotic targets has widely varying effects on growth. Proc Natl Acad Sci U S A 108, 4176–4181, doi:10.1073/pnas.1018301108 (2011). [PubMed: 21368134]

19. Xu W. et al. Chemical Genetic Interaction Profiling Reveals Determinants of Intrinsic Antibiotic Resistance in Mycobacterium tuberculosis. Antimicrob Agents Chemother 61, doi:10.1128/AAC.01334-17 (2017).
20. Pym AS et al. Regulation of catalase-peroxidase (KatG) expression, isoniazid sensitivity and virulence by furA of Mycobacterium tuberculosis. Mol Microbiol 40, 879–889 (2001). [PubMed: 11401695]
21. Zahrt TC, Song J, Siple J. & Deretic V. Mycobacterial FurA is a negative regulator of catalase-peroxidase gene katG. Mol Microbiol 39, 1174–1185 (2001). [PubMed: 11251835]
22. Zhang Y, Heym B, Allen B, Young D. & Cole S. The catalase-peroxidase gene and isoniazid resistance of Mycobacterium tuberculosis. Nature 358, 591–593, doi:10.1038/358591a0 (1992). [PubMed: 1501713]
23. Santangelo MP et al. Negative transcriptional regulation of the mce3 operon in Mycobacterium tuberculosis. Microbiology 148, 2997–3006, doi:10.1099/00221287-148-10-2997 (2002). [PubMed: 12368433]
24. Santangelo MP et al. Study of the role of Mce3R on the transcription of mce genes of Mycobacterium tuberculosis. BMC microbiology 8, 38, doi:10.1186/1471-2180-8-38 (2008). [PubMed: 18304349]
25. de la Paz Santangelo, M. et al. Mce3R, a TetR-type transcriptional repressor, controls the expression of a regulon involved in lipid metabolism in Mycobacterium tuberculosis. Microbiology 155, 2245–2255, doi:10.1099/mic.0.027086-0 (2009). [PubMed: 19389781]
26. Karakousis PC, Williams EP & Bishai WR Altered expression of isoniazid-regulated genes in drug-treated dormant Mycobacterium tuberculosis. The Journal of antimicrobial chemotherapy 61, 323–331, doi:10.1093/jac/dkm485 (2008). [PubMed: 18156607]
27. Vilcheze C. et al. Enhanced respiration prevents drug tolerance and drug resistance in Mycobacterium tuberculosis. Proc Natl Acad Sci U S A 114, 4495–4500, doi:10.1073/pnas.1704376114 (2017). [PubMed: 28396391]
28. Schoutrop ELM et al. The stability of antimycobacterial drugs in media used for drug susceptibility testing. Diagn Microbiol Infect Dis 92, 305–308, doi:10.1016/j.diagmicrobio.2018.06.015 (2018). [PubMed: 30025972]
29. Rouse DA, DeVito JA, Li Z, Byer H. & Morris SL Site-directed mutagenesis of the katG gene of Mycobacterium tuberculosis: effects on catalase-peroxidase activities and isoniazid resistance. Mol Microbiol 22, 583–592, doi:10.1046/j.1365-2958.1996.00133.x (1996). [PubMed: 8939440]
30. Liu Y. et al. Immune activation of the host cell induces drug tolerance in Mycobacterium tuberculosis both in vitro and in vivo. J Exp Med 213, 809–825, doi:10.1084/jem.20151248 (2016). [PubMed: 27114608]
31. Ma S. et al. Integrated Modeling of Gene Regulatory and Metabolic Networks in Mycobacterium tuberculosis. PLoS Comput Biol 11, e1004543, doi:10.1371/journal.pcbi.1004543 (2015). [PubMed: 26618656]
32. Mawuenyega KG et al. Mycobacterium tuberculosis functional network analysis by global subcellular protein profiling. Mol Biol Cell 16, 396–404, doi:10.1091/mbc.E04-04-0329 (2005). [PubMed: 15525680]
33. Raimunda D, Long JE, Padilla-Benavides T, Sassetti CM & Arguello JM Differential roles for the Co(2+) /Ni(2+) transporting ATPases, CtpD and CtpJ, in Mycobacterium tuberculosis virulence. Mol Microbiol 91, 185–197, doi:10.1111/mmi.12454 (2014). [PubMed: 24255990]
34. Lew JM, Kapopoulou A, Jones LM & Cole ST TubercuList--10 years after. Tuberculosis (Edinb) 91, 1–7, doi:S1472-9792(10)00111-3 [pii] 10.1016/j.tube.2010.09.008 (2011). [PubMed: 20980199]
35. Patel SJ et al. Fine-tuning of Substrate Affinity Leads to Alternative Roles of Mycobacterium tuberculosis Fe2+-ATPases. J Biol Chem 291, 11529–11539, doi:10.1074/jbc.M116.718239 (2016). [PubMed: 27022029]
36. Bulatovic VM et al. Oxidative stress increases susceptibility of Mycobacterium tuberculosis to isoniazid. Antimicrob Agents Chemother 46, 2765–2771 (2002). [PubMed: 12183226]

37. Slayden RA & Barry CE 3rd. The genetics and biochemistry of isoniazid resistance in mycobacterium tuberculosis. Microbes Infect 2, 659–669, doi:10.1016/s1286-4579(00)00359-2 (2000). [PubMed: 10884617]
38. Kohanski MA, Dwyer DJ, Hayete B, Lawrence CA & Collins JJ A common mechanism of cellular death induced by bactericidal antibiotics. Cell 130, 797–810, doi:10.1016/j.cell.2007.06.049 (2007). [PubMed: 17803904]
39. Hu J, Zhao L. & Yang M. A GntR family transcription factor positively regulates mycobacterial isoniazid resistance by controlling the expression of a putative permease. BMC microbiology 15, 214, doi:10.1186/s12866-015-0556-8 (2015). [PubMed: 26474554]
40. Zhou L, He ZG & Li W. AraR, an L-Arabinose-Responding Transcription Factor, Negatively Regulates Resistance of Mycobacterium smegmatis to Isoniazid. Biochemistry (Mosc) 84, 540–552, doi:10.1134/S0006297919050080 (2019). [PubMed: 31234768]
41. Ehrt S. et al. Controlling gene expression in mycobacteria with anhydrotetracycline and Tet repressor. Nucleic Acids Res 33, e21, doi:10.1093/nar/gni013 (2005). [PubMed: 15687379]
42. Ehrt S. & Schnappinger D. Controlling gene expression in mycobacteria. Future Microbiol 1, 177–184, doi:10.2217/17460913.1.2.177 (2006). [PubMed: 17661663]
43. Guo M. et al. Dissecting transcription regulatory pathways through a new bacterial one-hybrid reporter system. Genome Res 19, 1301–1308, doi:10.1101/gr.086595.108 (2009). [PubMed: 19228590]
44. Klotzsche M, Ehrt S. & Schnappinger D. Improved tetracycline repressors for gene silencing in mycobacteria. Nucleic Acids Res 37, 1778–1788, doi:10.1093/nar/gkp015 (2009). [PubMed: 19174563]
45. BEI Resources Strain Depository, <www.beiresources.org>
46. Rock JM et al. Programmable transcriptional repression in mycobacteria using an orthogonal CRISPR interference platform. Nat Microbiol 2, 16274, doi:10.1038/nmicrobiol.2016.274 (2017). [PubMed: 28165460]
47. Langmead B. & Salzberg SL Fast gapped-read alignment with Bowtie 2. Nat Methods 9, 357–359, doi:10.1038/nmeth.1923 (2012). [PubMed: 22388286]
48. Li H. et al. The Sequence Alignment/Map format and SAMtools. Bioinformatics 25, 2078–2079, doi:10.1093/bioinformatics/btp352 (2009). [PubMed: 19505943]
49. Ma S. et al. Transcriptomic Signatures Predict Regulators of Drug Synergy and Clinical Regimen Efficacy against Tuberculosis. mBio 10, e02627–02619, doi:10.1128/mBio.02627-19 (2019). [PubMed: 31719182]
50. Rustad TR, Harrell MI, Liao R. & Sherman DR The enduring hypoxic response of Mycobacterium tuberculosis. PLoS One 3, e1502, doi:10.1371/journal.pone.0001502 (2008). [PubMed: 18231589]
51. Nandakumar M, Prosser GA, de Carvalho LP & Rhee K. Metabolomics of Mycobacterium tuberculosis. Methods Mol Biol 1285, 105–115, doi:10.1007/978-1-4939-2450-9_6 (2015). [PubMed: 25779312]
52. Garcia BJ, Datta G, Davidson RM & Strong M. MycoBASE: expanding the functional annotation coverage of mycobacterial genomes. BMC Genomics 16, 1102, doi:10.1186/s12864-015-2311-9 (2015). [PubMed: 26704706]
53. Mi H. et al. PANTHER version 11: expanded annotation data from Gene Ontology and Reactome pathways, and data analysis tool enhancements. Nucleic Acids Res 45, D183–D189, doi:10.1093/nar/gkw1138 (2017). [PubMed: 27899595]

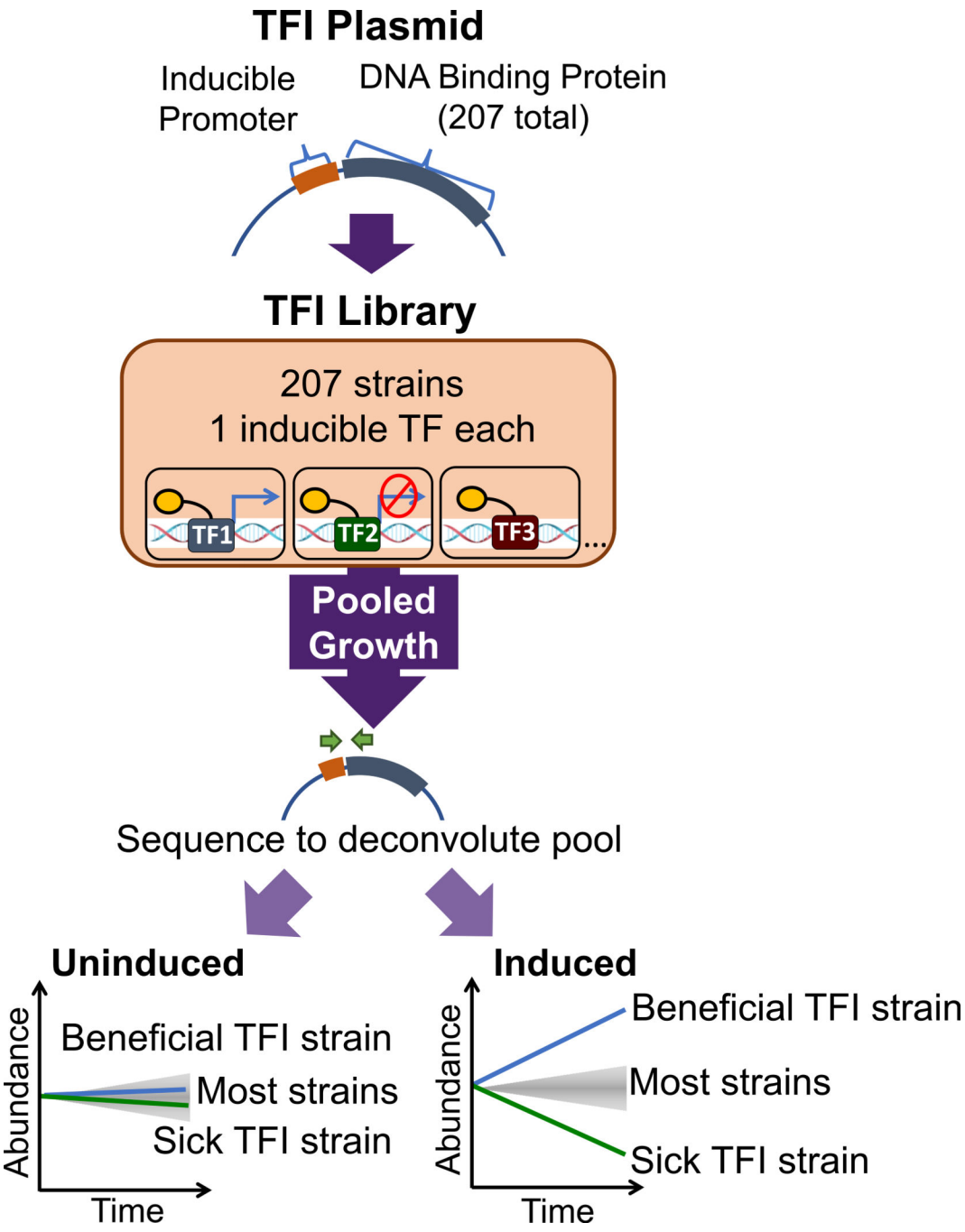

Figure 1.
Schematic of TRIP screen. See Methods for details.

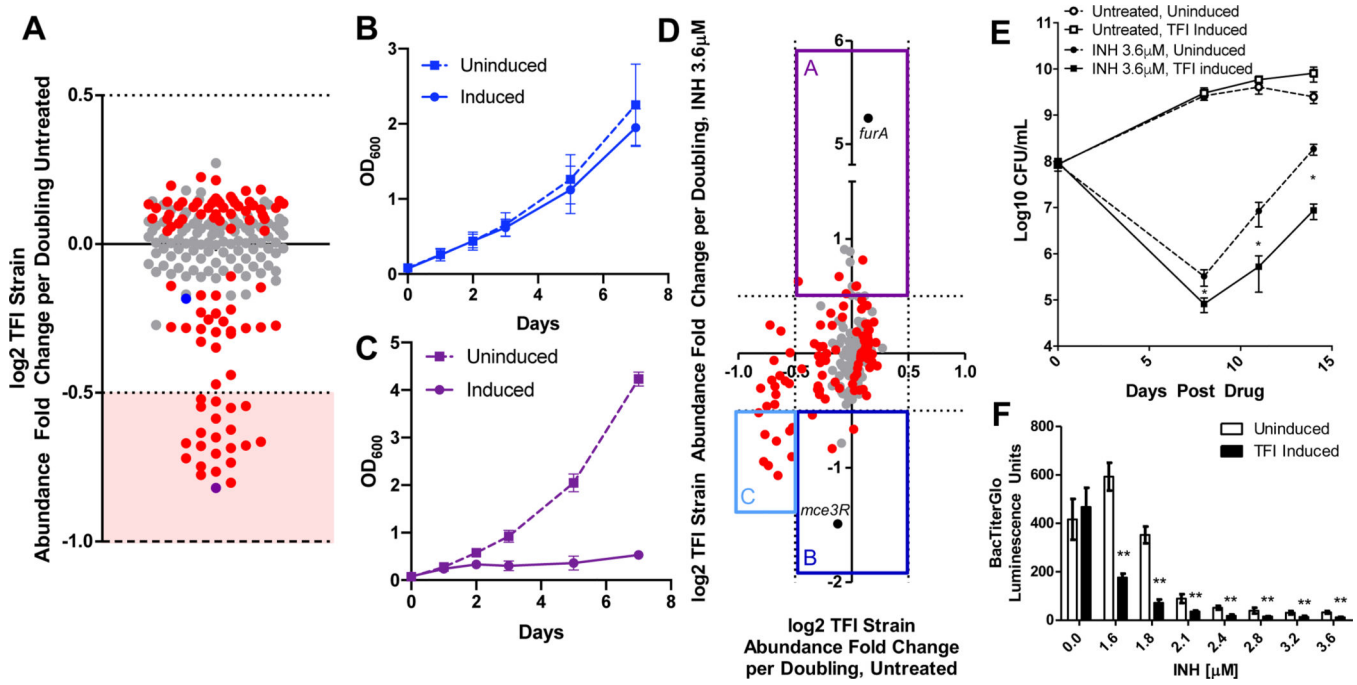

Figure 2. Regulon-mediated growth responses.

(A) Log-phase TRIP results. Dots represent mean abundance change of TFI strains induced vs. uninduced, normalized by the estimated number of pool doublings (averaged from four biological replicates). Red dots indicate z-score > 1, calculated from four replicates. Dotted lines specify ± 2 standard deviations, and dashed line denotes detection limit, signifying no growth. Shaded area represents strains with strong defects. Monoculture growth curves of two strains (blue, purple dots) are shown in (B) and (C) respectively, with induction (solid) or without (dashed). Data show mean ± standard deviation (SD) of three biological replicates from three independent experiments. (D) TRIP results with INH (y-axis) vs. no drug (x-axis) (each dot represents a mean of four biological replicates). Since INH can be bactericidal, some strains showed abundance changes < −1. Boxes demarcate strains with altered INH survival. Black dots represent strains: *furA* (*furA*$_{ind}$) and *mce3R* (*mce3R*$_{ind}$). (E) *mce3R*$_{ind}$ colony forming units (CFU)/mL over 14 days in INH (black) vs. no drug (white) with induction (solid) or without (dashed). Data show mean ± SD of three biological replicates from one representative experiment (the experiment was performed independently three times) ($p = 0.00012$, two-sided t-test comparing Uninduced vs. TFI-induced in INH, day 8; $p = 0.015$, two-sided t-test comparing Uninduced vs. TFI-induced in INH, day 11; $p = 7.0 \times 10^{-8}$, two-sided t-test comparing Uninduced vs. TFI-induced in INH, day 14). (F) *mce3R*$_{ind}$ metabolic viability after 7 days INH with induction (black) or without (white), measured by luminescence (see Methods). Data show mean ± SD of four biological replicates from one representative experiment (the experiment was performed independently three times). See Extended Data 3 for a version of panel (F) with the individual replicates visualized and the exact p-values for each individual comparison enumerated. * and ** indicate significant differences between induction states ($p < 0.05$ and $p < 0.001$, two-sided t-test, respectively).

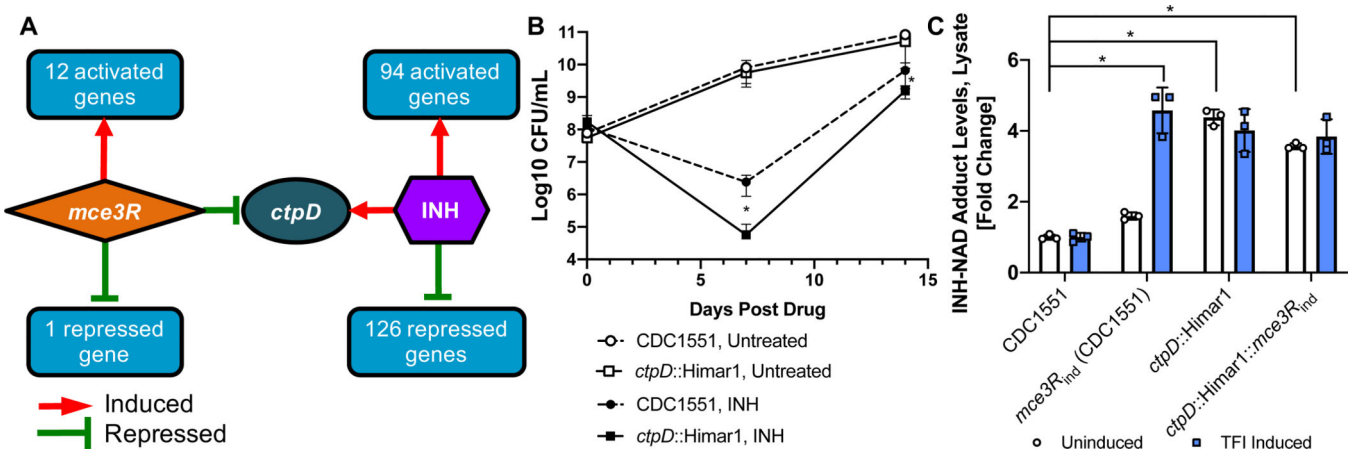

Figure 3. *mce3R* regulon reveals effector of INH susceptibility.

(A) Network representation of overlap between *mce3R* regulon and genes differentially expressed in wildtype response to INH exposure. Red arrows indicate genes activated at least 2-fold, and green lines indicate genes repressed at least 2-fold. (B) CFU/mL over 14 days of *ctpD*::Himar1 transposon disruption strain (solid) compared to the wildtype strain, CDC1551 (dashed). Both strains were exposed to 3.6μM INH (black) vs. no drug (white). Data show mean ± SD from three biological replicates of one representative experiment (the experiment was performed independently three times) ($p = 0.0021$, two-sided t-test for CDC1551 + INH day 7 vs. *ctpD*::Himar1 + INH day 7; $p = 0.029$, two-sided t-test for CDC1551 + INH day 14 vs. *ctpD*::Himar1 + INH day 14). (C) Mass spectrometry quantification of relative intracellular INH-NAD adduct levels in the $mce3R_{ind}$ and *ctpD*::Himar1 strains after 24 hours of exposure to 7.2 μM INH show elevated INH-NAD levels relative to wildtype. There is no significant difference between INH-NAD levels in *ctpD*::Himar1 strain with and without *mce3R* induction. Data show mean ± SD of three biological replicates from one representative experiment (the experiment was performed independently two times) ($p = 0.00067$, two-sided t-test comparing CDC1551 vs. $mce3R_{ind}$ (CDC1551) TFI induced; $p = 0.000015$, two-sided t-test comparing CDC1551 vs. *ctpD*::Himar1; $p = 0.00057$, two-sided t-test comparing CDC1551 vs. *ctpD*::Himar1::$mce3R_{ind}$ TFI induced; $p = 0.16$, two-sided t-test comparing *ctpD*::Himar1 vs. *ctpD*::Himar1::$mce3R_{ind}$ TFI induced).